Eur Food Res Technol (2011) 232:693–702
DOI 10.1007/s00217-011-1438-4

ORIGINAL PAPER

Soluble starch–based biodegradable and microporous microspheres as potential adsorbent for stabilization and controlled release of coix seed oil

Hailong Peng · Hua Xiong · Shenqi Wang · Jinhua Li · Lingxin Chen · Qiang Zhao

Received: 2 November 2010 / Revised: 11 January 2011 / Accepted: 17 January 2011 / Published online: 5 February 2011

Abstract Soluble starch–based biodegradable and microporous microspheres (SDM-Ms) were prepared by emulsion chemical cross-linking technique using trisodium trimetaphosphate (TSTP) as the cross-linker. The resultant amorphous SDM-Ms were excellently identified by scanning electron microscopy (SEM), X-ray diffraction (XRD), and Fourier transform infrared spectroscopy (FT-IR). The internal rupture and surface-controlled erosion were the predominant degradation mechanisms for SDM-Ms. The obtained SDM-Ms were applied to adsorb coix seed oil (CSO) by immersing method. The adsorption capacity of CSO within SDM-Ms was determined, namely 0.5238 g/g, and the thermal stability was shown higher than that of the free CSO. A burst release appeared in the second hour, followed by controlled release. Diffusion, degradation, and erosion mechanisms might coexist for the full release processes. The soluble starch (Ss) was demonstrated a promising biodegradable polymer for preparing the porous microspheres. Meanwhile, after being adsorbed into the SDM-Ms, the CSO can be powerfully applied in food and pharmaceutical industries.

Keywords Soluble starch · Microspheres · Thermal stability · Adsorption capacity · Release mechanisms · Coix seed oil

H. Peng · H. Xiong (✉) · S. Wang · Q. Zhao
State Key Laboratory of Food Science and Technology, Nanchang University, 330047 Nanchang, Jiangxi, China
e-mail: huaxiong100@yahoo.com.cn

H. Peng
Department of Chemical and Pharmaceutical Engineering, Nanchang University, 330031 Nanchang, Jiangxi, China

J. Li · L. Chen
Key Laboratory of Coastal Zone Environmental Processes, CAS, Yantai, China

J. Li · L. Chen
Shandong Provincial Key Laboratory of Coastal Zone Environmental Processes, CAS, Yantai, China

J. Li · L. Chen
Yantai Institute of Coastal Zone Research, Chinese Academy of Sciences, 264003 Yantai, China

Introduction

Coix seed oil (CSO), obtained from coix seed (*Coix lacryma-jobi L. var. ma-yue Stapf*), has been used as traditional Chinese medicine, nourishing food sources, and supplements for a long time [1] in Asian countries. It is well known that CSO possesses diverse antitumor activities and has been widely applied to treat multiple primary malignant tumors [2, 3]. Furthermore, CSO has various exceptional properties of enhancing the immunocompetence and effect of natural killer cells on tumor cells [4], and help prevent the decrease in white blood cells during chemical therapy [5, 6]. However, it also has some drawbacks, involving biological instability, poor water-solubility, low adsorption capacity, and short biological half time in body, which restrict the utilization of CSO in food and pharmaceutical industries. In order to overcome these disadvantages, CSO is encapsulated into liposome and emulsions. Unfortunately, liposome suspensions and emulsions are subjected to a series of problems such as aggregation, fusion, and lower loading capacity. One effective approach to address these problems is to formulate aqueous preparations into solid ones. Loading of CSO

into the solid biodegradable microspheres might be one of the potential novel methods.

Biodegradable microspheres have been extensively used in pharmaceutical industry because of its advantages of protecting stability, controlled release, decreasing toxicity, and improving biological half time for bioactive agents [7, 8]. Biodegradable polymers were the key factor for preparation of biodegradable microspheres, among which, synthetic biodegradable polymers occupy predominant roles and their applications have been dramatically expanded in the past decades [9]. However, they were associated with two shortcomings. On the one hand, the synthetic polymers have considerable toxicity and can cause safety risks. On the other hand, the complex synthesis route of polymers would lead to high cost and environmental pollutions. As is known to all, the ideal biodegradable polymers should be characterized by their ability to degrade into nontoxic end products in vivo situation and could be eventually eliminated from organism. Therefore, it is necessary and crucial to search for novel biodegradable polymers for microspheres, and the natural polymers are being received great concern from researchers increasingly.

Starch is the most abundant reserve carbohydrate in plants, especially present in many farm products such as rice, wheat, maize, and potatoes [10, 11]. Starches have been widely used due to their attractive characteristics of biocompatibility, biodegradability, nontoxicity, abundance, low cost, edibility, good adsorbing, and film forming ability [12, 13] in food, pharmaceutical, and environmental industries. However, most starch is only used for edible or producing low value-added products, which easily leads to accumulation, quality decrease, resources waste, and economic loss for starches. So, exploring novel applications and high value-added products, to meet the increasing demand and overcome current price limitations of starches, has become very significant. To the best of our knowledge, there are few reports on the utilization of soluble starch (Ss) as biodegradable polymers for producing microporous microspheres.

In this work, soluble starch–based biodegradable and microporous microspheres (SDM-Ms) were prepared by emulsion cross-linking method using trisodium trimetaphosphate (TSTP) as crosslinker. Meanwhile, SDM-Ms were applied to adsorbing CSO. Scanning electron microscopy (SEM), X-ray diffraction (XRD), and Fourier transform infrared spectroscopy (FT-IR) were all employed to characterize SDM-Ms. The degradation processes and mechanism were determined by optical microscope and mass loss, respectively. Furthermore, the thermal stability and in vitro release properties of CSO within SDM-Ms were also studied in detail.

Materials and methods

Materials

Soluble starch (Ss) was kindly supplied by Nantong Luo Gai Te Biotechnology Co., Ltd. (Nantong, China). Coix seed oil (CSO) was purchased from Hecheng Sanxian Biotechnologies Co., Ltd. (Guangzhou, China). Trisodium trimetaphosphate (TSTP) was donated by Hong Rui Chemical import and export Co., Ltd. (Nanjing, China). Liquid paraffin, span 80 and tween 80 were both purchased from Sinopharm Chemical Reagent Co., Ltd. (Shanghai, China). All the chemical agents used were of analytical grade.

Preparation of microspheres

SDM-Ms were prepared via emulsion (water in oil, w/o) chemical cross-linking method [14, 15]. TSTP was used as the cross-linker because it is a solid of low toxicity with no adverse effects on humans. Ss and TSTP were mixed in sodium hydroxide (NaOH) aqueous solution (5 mL, 0.5 M) with stirring for 3 min, which was used as the water phase. Liquid paraffin (50 mL) containing 2% (v/v) span 80 and tween 80 (1:1, v/v) emulsifier was used as the oil phase. Then, the water phase (5 mL) were added drop wise into the oil phase (50 mL) by an injector, and the cross-linking reaction took place at 45 °C with a constant stirring at the speed of 400 rpm for 5 h. The obtained SDM-Ms were collected and washed three times with petroleum ether, acetone ethanol, and deionized water, respectively. Finally, the products were dried in a vacuum oven at 45 °C for 12 h and kept in desiccators for further analysis.

Scanning electron microscopy (SEM)

The samples were sprinkled onto a double-sided tape, and the morphological features were examined by scanning electron microscopy (SEM) (Quanta 200F, FEI, Hillsboro, OR, USA). The inner structures of SDM-Ms were also observed after fracturing microspheres using a razor blade.

Fourier transform infrared spectroscopy (FT-IR)

Fourier transform infrared spectroscopy (FT-IR) spectra were recorded by using a Spectrophotometer (Nicolet 5700, Thermo Electron Corporation, MA, USA). Ss and SDM-Ms samples were prepared by processing compressed KBr disks. Spectra were scanned in the range between 4,000 and 500 cm^{-1}.

X-ray diffraction (XRD)

The X-ray diffraction (XRD) pattern was recorded using XRD analyser (D8-focus, Bruker, Karlsruhe, Germany)

with the scattering angle (2θ) range of 2–60 °C. Ss, SDM-Ms and TSTP were together packed tightly in sample holders with Cu radiation at 40 kV, 40 mA, and 0.4 s/min running velocity.

In vitro degradation

In vitro degradation studies were performed according to the methods developed by Hamdi et al. [16]. SDM-Ms (0.5 g) were added into phosphate buffer (pH 7.4, 50 mL) containing α-amylase (0.25 g) with mild agitation and incubated at 37 °C. At predetermined time, samples were withdrawn and dried. The morphology of SDM-Ms after degradation was studied by optical microscope. Meanwhile, the Prout–Tompkins equation [17] and mass loss (ML) were determined for studying the degree of degradation based on the following equations:

$$\mathrm{ML}\,(\%) = [(W_0 - W_t)/W_0] \times 100$$

$$\ln[(1 - \mathrm{ML})/\mathrm{ML}] = K_d t + m$$

$$m = -K_d t_{50}$$

where W_0 and W_t are the weight of SDM-Ms before and after incubation, respectively, K_d (h^{-1}) is the rate constant, and t_{50} (h) is the time to achieve 50% ML.

Adsorption capacity (AC)

A certain amount of SDM-Ms (1 g) were added into CSO (5 g) and mixed for 30 min, and then incubated in shadow for 24 h at room temperature. Oleic acid (OA) in the CSO solution was used as the parameter to determine adsorption capacity of CSO in the SDM-Ms by high-performance liquid chromatography (HPLC) method [18] at the wavelength of 254 nm. The analytical column was a C_{18} column (5-μm particles, 4.6 × 150 mm, Waters, Milford, MA, USA). The mobile phase consisted of acetonitrile/tetrahydrofuran/water (78:2:20, v/v/v) at a flow rate of 1.0 mL min^{-1} and the volume of injection was 20 μL at 30 °C. Then, adsorption capacity (AC) was calculated using the following equation:

$$\mathrm{AC}\,(\%) = [(W_i - W_a)/W_s] \times 100$$

where W_a and W_i are the weight of OA after adsorption and initial addition, respectively, and W_s is the weight of SDM-Ms.

Thermal stability

The thermal stabilities of free CSO and SDM-Ms after adsorbing CSO were determined using differential scanning calorimeter (SDT-Q-600, TGA-DSC, TA instruments, USA) in nitrogen environment. The samples were conditioned on hermetic aluminum pans and heated at rising rate of 5 °C min^{-1} in the range of 50–600 or 800 °C.

In vitro release

SDM-Ms (0.1 g) were placed into glass test tubes containing gastric fluid (2 mL, pH 1.2) or intestinal fluid (2 mL, pH 7.5), respectively. The release media were incubated at 37 ± 0.1 °C. At predetermined time, samples from each test tube were drawn and placed at a Whatman No. 1 filter paper to adsorb the released CSO. The filter papers were then dried, and the released CSO contents were measured. And the amount of CSO released from SDM-Ms was calculated as a percentage of the initial amount of CSO incorporated in SDM-Ms prior to incubation test.

In vitro release mechanism

In order to investigate and decouple the release mechanism for CSO from SDM-Ms, the release profiles were calculated using different models [19]:

Zero-order model: $M_t/M_\infty = kt$
First-order model: $\ln\,(1 - M_t/M_\infty) = -kt$
Higuchi model: $M_t/M_\infty = kt^{1/2}$
Peppas model: $\ln M_t/M_\infty = n \ln t + \ln k$

where M_t/M_∞ is the fractional active agents release at time t, k is a constant incorporating the properties, and n gives an indication of the release mechanism.

Fickian diffusion and erosion are the dominant release mechanisms for microsphere. So, Peppas and Sahlin model [19] was used to investigate the release mechanisms at different stages:

Peppas and Sahlin models: $M_t/M_\infty = K_1 t^m + K_2 t^{2m}$

where K_1 is the Fickian kinetic constant, K_2 is the erosion rate constant, and the value of m was 0.5.

Results and discussion

Morphology

Figure 1 shows the morphology of SDM-Ms using SEM. Smooth surface and spherical shapes with aggregation are exhibited (Fig. 1a, b). The phenomenon of aggregation was mainly attributed to the results of the emulsification and cross-linking process. Previous studies [14, 20] reported that the size distribution of the droplets in the emulsion was wide when emulsified by mechanical stirring, which led to the aggregation and breakup of droplets during the emulsification and cross-linking process. So, the phenomenon of

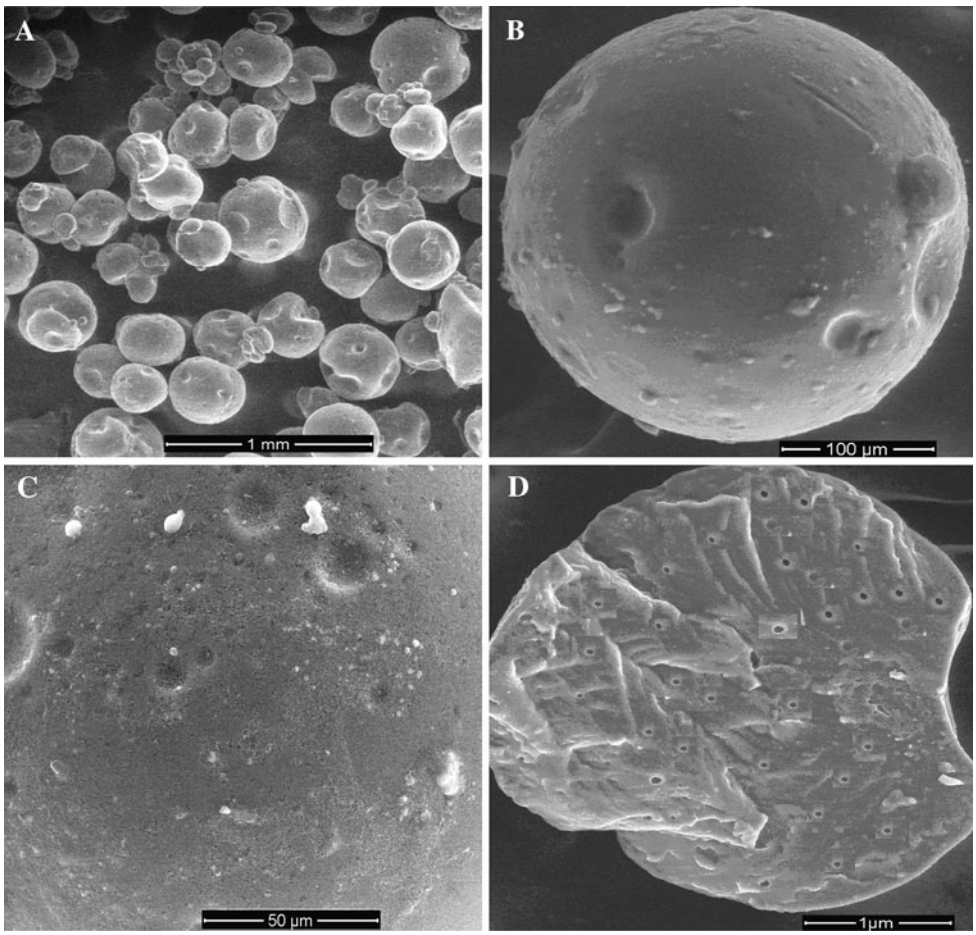

Fig. 1 SEM images of SDM-Ms

aggregation between SDM-Ms would appear. Meanwhile, van der Waals force and electrostatic attraction may also play important roles for particles aggregation. The surfaces and the internal structure of SDM-Ms have a compacted and continuous network with certain microporosities (Fig. 1c, d). The formation of microporosities may be related to the mechanisms of air bubbles or entrapped organic solvent evaporating during the cross-linking and drying processes [21]. The evaporation of solvent after drying in microspheres also leads to the shrinkage of interior porous structure compared with the optical microscope photographs, but still retained to a certain extent. The microporosities of microspheres are the key factor for adsorption capacity and release rate of bioactive agents. Thus, the number and size of micropore should be confirmed and optimized when preparing microspheres.

Fourier transform infrared spectroscopy (FT-IR)

Fourier transform infrared spectroscopy (FT-IR) was used to confirm the structural organization of SDM-Ms after cross-linking. FT-IR spectra are shown in Fig. 2 for Ss and SDM-Ms. In the FT-IR spectrum of Ss (Fig. 2a), the presence of –O–H is confirmed due to stretching vibration at 3,383.01 cm^{-1}, and the peak at 1,247.83 cm^{-1} corresponds to –O–H bending vibration. The bands in the region 1,413.04–1,367.23 cm^{-1} are attributed to –C–H bending vibrations, and the one observed at 2,930.18 cm^{-1} is due to –C–H stretching vibrations. The bands at 1,156.52 cm^{-1} are due to C–O stretching vibrations. Figure 2b shows the FT-IR spectrum of SDM-Ms. As can be seen, the main vibrations of –O–H, –C–H, and C–O have no significant changes between SDM-Ms and Ss. The broad band at 3,383.82 cm^{-1} shows lower intensity compared with Ss. However, it is interesting that the characteristic peaks of P=O (1,210 cm^{-1}) and P–O–C (810 cm^{-1}) do not appear in the FT-IR spectrum of SDM-Ms, which may be due to the very low cross-linking degree for SDM-Ms. Thus, the characteristic peaks of P=O and P–O–C could not be detected by the FT-IR.

However, the FT-IR spectrum of SDM-Ms has its super properties compared with Ss. The band of 1,062.61 cm^{-1} disappeared, and the band at 929.75 cm^{-1} became weaker. On the contrary, the band at 1,022.79 cm^{-1} became larger and stronger. The band of 1,062 and 930 cm^{-1} may be related to crystal organization for Ss, and the peak area of

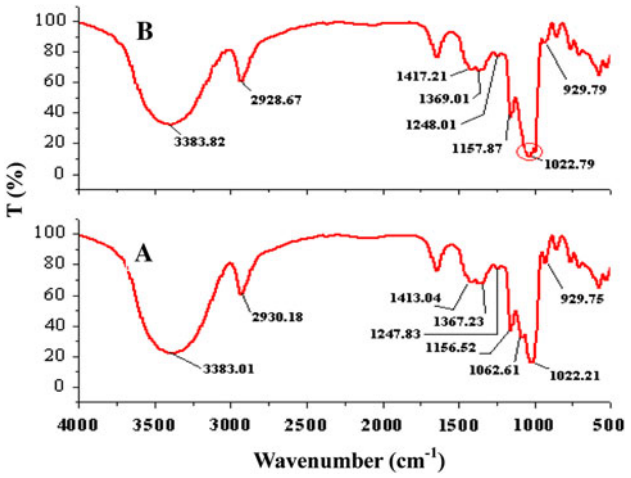

Fig. 2 FT-IR spectrum of Ss (**a**) and SDM-Ms (**b**)

(1,062 + 930) cm^{-1} would be decreased with the crystallinity decreasing. The changes of 1,022 cm^{-1} represented the changes of amorphous morphology for Ss, and the peak area of 1,022 cm^{-1} would be increased when the crystallinity decreased. So, the changes of crystallinity could be explained by the absorbance ratio of (1,062 + 930) and 1,022 cm^{-1}. The morphology of Ss had been changed from angular to round shape with the absorbance ratio (1,062 + 930)/1,022 cm^{-1} decreasing after cross-linking, all of which indicated that the structural organization of Ss had been changed from crystalline into amorphous after cross-linking reaction. This finding was different from that reported by Ispas-Szabo [22], where the absorbance ratio of (1,047 + 980) and 1,022 cm^{-1} was considered to represent the changes of crystalline starch. This difference may result from the diversity of starch.

X-ray diffraction (XRD)

The XRD patterns of TSTP, Ss, and SDM-Ms are shown in Fig. 3. TSTP shows intense peaks of 2θ between 10° and 60° (Fig. 3a), which indicated that TSTP has its property of crystalline nature. This result was consistent with that reported by Li et al. [14]. In the XRD of Ss (Fig. 3b), the typical C-type XRD pattern [23] with strong peaks at 2θ close to 5.65°, 14.20°, 17.37°, 18.70°, and 23.37° was observed, which is may be the results of crystalline regions in the Ss. However, the crystallinity is dramatically reduced after cross-linking (Fig. 3c). This loss in crystallinity may be attributed to the effect of the alkaline environment and the rupture/breakage of chemical bonds in Ss molecules during the cross-linking process. Weak and strong peaks appeared at 2θ of 13.00° and 20.60° for the SDM-Ms (Fig. 3c), respectively. The results of XRD suggested that the structure of Ss was changed from crystalline into amorphous, which was in agreement with the results of

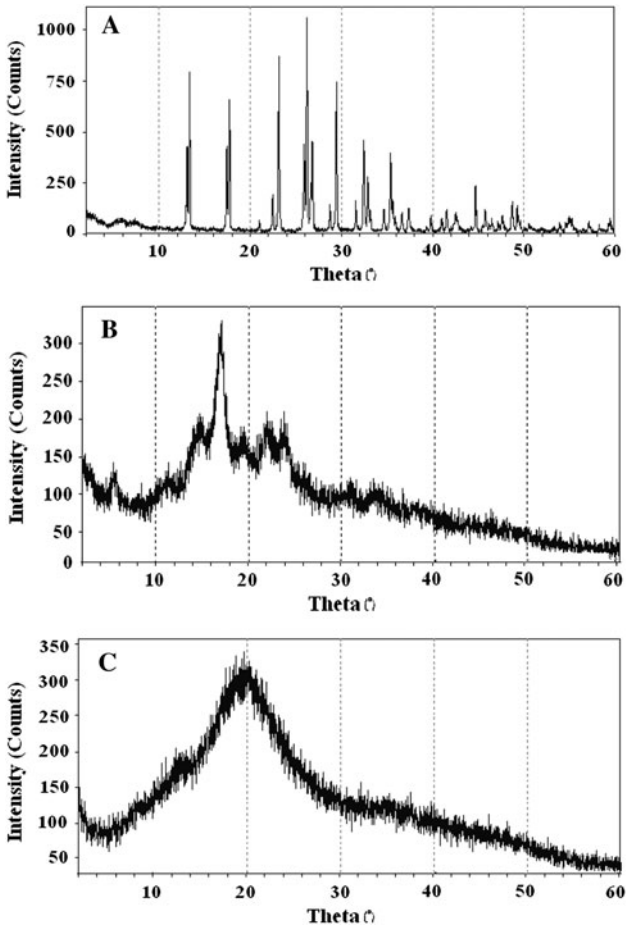

Fig. 3 XRD patterns of TSTP (**a**), Ss (**b**), and SDM-Ms(**c**)

FT-IR. The adsorption capacity would be increased with the increase of the amorphous structures of starch. Thus, the adsorption capacity of SDM-Ms was higher than that of Ss.

In vitro degradation

The optical morphology changes of SDM-Ms at degradation time of 1, 2, 3, 6, 9, and 15 h are shown in Fig. 4a–f, respectively. By contrast with the morphology of initial microspheres, the SDM-Ms is almost maintained spherical shape after 1-h degradation (Fig. 4a). However, it is obvious that the microporous pores became into mesopores on the surface of SDM-Ms after 2-h degradation (Fig. 4b), which might because that water was penetrated into SDM-Ms through the microporous pores and hydrolysis took place on the wall of microporous pores with dissolution and diffusion of monomers. Notably, the SDM-Ms showed coarse surfaces with the meso-pores size increasing greatly during 3 h of degradation (Fig. 4c). This was probably owing to the increase of the degree of crystallinity of Ss

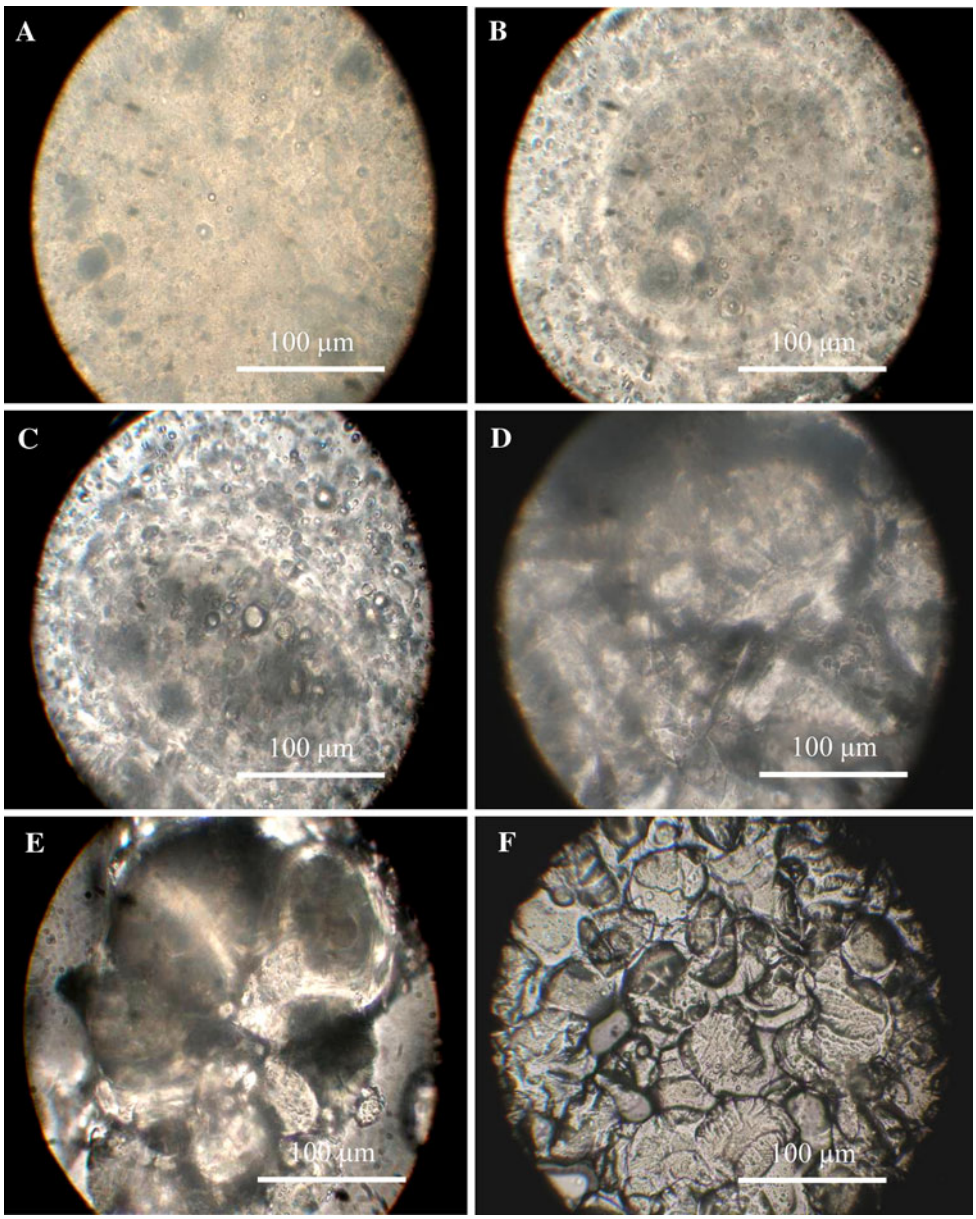

Fig. 4 Optical microphotograph of SDM-Ms (**a–f**) degraded at 1, 2, 3, 6, 9, and 15 h, respectively

and the beginning of surface-controlled erosion of SDM-Ms, which induced the shrinkage of the microspheres surface. After 6-h degradation, the shell layer starch fell off from SDM-Ms surface gradually (Fig. 4d). At that time, the diffusion rate of α-amylase into the SDM-Ms was slower and decreased, which led a large number of α-amylases to attack the surface of SDM-Ms and the degree of erosion became stronger (that is the liquid–solid interface degradation). The limitation of α-amylase into the SDM-Ms may result from two factors. The first one is that the α-amylase binding to the substrate would slow down the diffusion process, especially under unsaturated conditions. The second one is that successful diffusion of α-amylase into the swollen SDM-Ms requires the presence of sufficiently large pores. The SDM-Ms lost their spherical structure (Fig. 4e) after 9-h degradation, and the structures of SDM-Ms have been destroyed by α-amylase and degraded absolutely in the following time (Fig. 4f). The internal rupture of SDM-Ms occurred, and the discrete fragments were formed. It is recognized that the degradation of SDM-Ms induced by α-amylase occurs in three steps: (1) surface-controlled erosion of the SDM-Ms, (2) diffusion of the enzyme molecules through the SDM-Ms, and (3) surface-controlled erosion and internal rupture occurring simultaneously.

In order to gain insight into the degree of degradation, the mass loss (ML) of SDM-Ms was investigated. Obviously, the ML was negligible during the 2-h degradation with ML of 2.55%. The ML was about 11.99% after 3-h degradation, then followed by a quick decreasing of

SDM-Ms mass over the next time, and the ML was up to 74.84%. The ML results were corresponded to the observation of morphology of degradable products. The Prout-Tompkins equation was also applied to investigate the degradation mechanism for SDM-Ms because the rate constant (K_d), and the time to obtain 50% of ML (t_{50}) were employed to represent the induction and acceleration of microspheres degradation. The K_d and t_{50} were -0.4063 h^{-1} and 10.59 h for SDM-Ms, respectively. It is evident that Ss was a biodegradable polymer for microspheres. The preparation conditions could be adjusted according to t_{50} for satisfying the requirement of bioactive agents release from microspheres in vitro or in vivo.

Adsorption capacity (AC)

The CSO was adsorbed into the solid SDM-Ms by a simple immersing method, and the AC was up to 0.5238 g/g. The CSO possesses many groups of –COOH and double bonds, leading to forming hydrogen bond and electrostatic interaction with SDM-Ms, all of which could improve the AC for SDM-Ms.

Adsorbing of bioactive agents into the biodegradable microspheres is a complicated physicochemical process. On the one hand, there are some micropores on the surface and internal structure of SDM-Ms (Fig. 1c, d), and those micropores formed mass-transfer channels. Bioactive agents could enter into the interior of SDM-Ms via mass-transfer channel under the driving of osmotic pressure. The electrostatic and hydrophobic interaction between SDM-Ms and bioactive agents also play important roles for AC. Meanwhile, the microsize, larger specific surface area, and energy of SDM-Ms would also improve the AC. All those above belong to the physical mechanism. On the other hand, chemical interaction between SDM-Ms and bioactive agents is the second mechanism for adsorbing capacity. The SDM-Ms has many groups of –OH, which could form hydrogen bond interaction with bioactive agents. The physicochemical adsorption mechanism occupies many advantages for SDM-Ms, such as simple processes, high adsorbing capacity, and mild conditions which could protect the activity of bioactive agents during adsorption processes.

Thermal analysis

The TGA-DSC curves of free and adsorbed CSO in SDM-Ms are shown in Fig. 5. DSC analysis of free CSO (Fig. 5a) shows a strong endothermic peak at 417.80 °C, which is due to the degradation of free CSO. The results were also confirmed by TGA curves, namely the free CSO decomposition in a single-stage reaction. The onset thermal degradation temperature of the free CSO is about 200.00 °C and the thermogravimetric loss was terminated at 473.98 °C. However, four strong endothermic peaks were found in the DSC curves of CSO after adsorbed into SDM-Ms (Fig. 5b). The first endothermic peak appeared at 58.56 °C, which may be because of the loss of water in SDM-Ms. The second and third endothermic peaks were at about 147.00 and 279.18 °C, respectively, which are attributed to the fraction of hydroxyl groups and decomposition of Ss. The fourth endothermic peak at 470.24 °C is due to the degradation of the adsorbed CSO. The TGA curve results suggested that there were three overlapping steps of degradation for SDM-Ms after adsorbing CSO. The first step in the range of 100.00–200.00 °C was related to evaporation of residual water in SDM-Ms. The second step in the range of 200.00–350.00 °C may be due to the degradation of Ss. The third one in the range of 350.00–560.00 °C was originated from the decomposition of CSO in the SDM-Ms. As can be seen that the initial degradation temperature of CSO increased from 200.00 to 350.00 °C after adsorbing into SDM-Ms. These results showed that the adsorbed CSO had significantly higher thermal stability and longer shelf life than that of the free CSO.

In vitro release

Figure 6 displays the cumulative release of CSO from SDM-Ms in intestinal and gastric fluid. A burst release rate was observed in the beginning of 2-h incubation and no significant difference occurred between the intestinal and gastric fluid. The phenomenon of burst release might be due to the diffusion of CSO on the surface and outside micropores of SDM-Ms. At the following time, a slower release appeared and only about 63.87 and 87.65% of CSO was released from SDM-Ms in the intestinal and gastric fluid after 18-h incubation, respectively. The reasons of a slower release may be due to the slowing degradation and erosion of SDM-Ms. The results also indicated that the release rate of CSO in intestinal fluid was higher than that in gastric fluid. This may be the difference of hydrolysis mechanisms in intestinal and gastric fluid. The fact is that H^+ and amylase hydrolysis reaction mechanism play predominant roles for SDM-Ms in gastric and intestinal fluid, respectively.

Release mechanism

For zero-order, first-order, Higuchi, Peppas, and Peppas and Sahlin models, the correlation coefficient (r^2) of linear relationship between the cumulative release and time was established for the evaluation of the release mechanism. From the results of Table 1, it can be observed that Peppas and Sahlin model was the most suitable model for describing CSO release kinetics from SDM-Ms because of

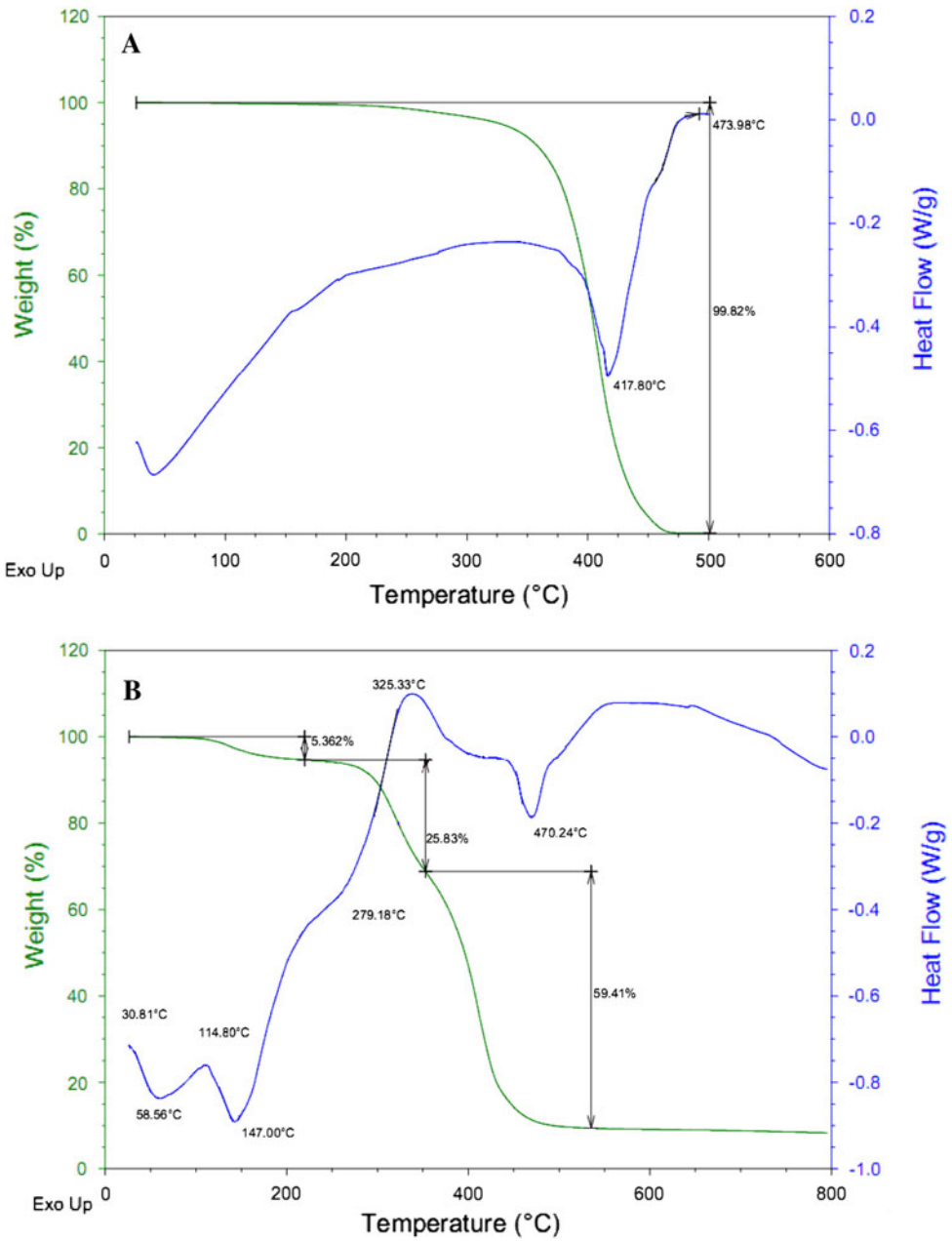

Fig. 5 TGA (*blue line*) and DSC (*green line*) curves of free CSO (**a**) and adsorbed CSO (**b**) in SDM-Ms

r^2 greater than that of other models. For gaining insight into the release mechanism of CSO from SDM-Ms at different release stages (i.e., burst and slower release process), K_1 and K_2 of Peppas and Sahlin model were fitted. At the burst release stage, the values of K_1 were 7.48 and 9.45 in the intestinal and gastric fluid media, and the values of K_2 were 7.93 and 8.48, respectively. Accordingly, the values of K_1 were 18.03 and 19.77, and the ones of K_2 were −0.35 and 0.88 at the slower release processes, respectively. Previous study [24, 25] reported that the release would occur predominantly by Fickian diffusion when the ratio of the diffusion to erosion (K_1/K_2) is greater than 1. When the ratio is less than 1, the release will occur predominantly by erosion. The results of this study indicated there is no great difference between the values of K_1 and K_2 for the burst release stage, implying that the mechanism of the CSO release from SDM-Ms occurred dominantly based on the Fickian diffusion and erosion. While diffusion is the main mechanism for the slower release stage because the values of K_1 were much greater than K_2, the fitting release of CSO from SDM-Ms was calculated according to Peppas and Sahlin model, where little difference was found between the experimental and fitting release results as shown in Fig. 7.

The release mechanism of CSO from SDM-Ms is schematically illustrated in Fig. 8. The concentration of CSO is higher at the local of SDM-Ms surface and outside

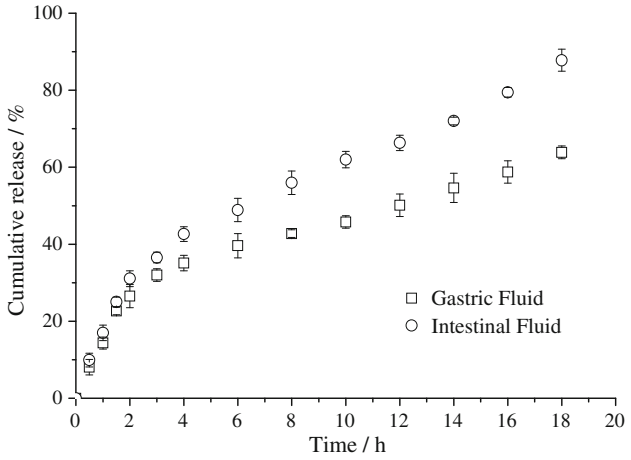

Fig. 6 In vitro release profiles of CSO from SDM-Ms in the intestinal and gastric fluid media

Table 1 Correlation coefficients (r^2) according to the different models used for describing CSO release mechanisms from SDM-Ms in the intestinal and gastric fluid media

Model	Intestinal fluid media		Gastric fluid media	
	Stage 1 r^2	Stage 2 r^2	Stage 1 r^2	Stage 2 r^2
Zero-order	0.94	0.99	0.95	0.99
First-order	0.96	0.98	0.97	0.92
Higuchi	0.98	0.97	0.98	0.98
Peppas	0.98	0.97	0.99	0.98
Peppas and Sahlin	0.99	1.00	0.99	0.99

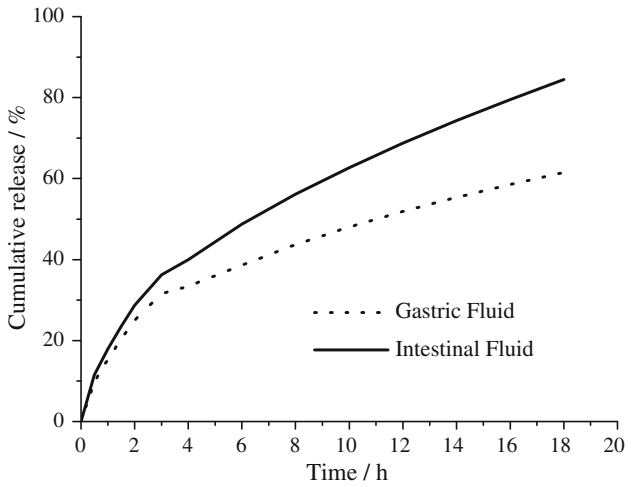

Fig. 7 The fitting profiles of the CSO release from SDM-Ms using Peppas and Sahlin model

micropores at the initial time. At that stage, Fickian diffusion governs the release mechanism and leads to burst release. Following the initial time (slower release stage),

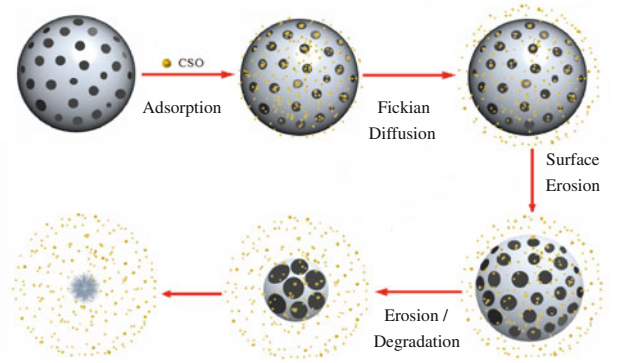

Fig. 8 Schematic illustration of CSO release from SDM-Ms

CSO on the surface was released completely and the interior CSO of the SDM-Ms was hindered by the macromolecular chains. At that time, the release mediums infiltrated gradually into the interior of SDM-Ms through multiple micropores and attacked the surfaces with the hydrolysis reaction of macromolecular chains occurring, which led to the bond rupture and degradation of SDM-Ms. Consequently, the structure of SDM-Ms was destroyed and the weight decreased, which is the erosion processes. Meanwhile, the micropores became bigger increasingly, and CSO could be diffused into mediums under the impelling of mediums via porosities. It is suggested that diffusion and erosion were the rate-limiting step for the release rate of CSO from SDM-Ms at slower release stage.

Usually, the empirical models, such as zero-order, first-order, Higuchi, Hixson-Crowell, and Peppas models, were applied to evaluate the release behaviors of bioactive agents from microspheres. However, the empirical models have disadvantages of neglecting the influence of transmitting phenomena of release mediums and the degradation changes of polymers during the release processes, which limits the application ranges and effectiveness of empirical models for describing the real release behaviors. Therefore, more studies are needed in order to achieve the mechanism models that are desired for describing the real release behaviors.

Conclusions

In the present work, the production of porous microspheres made from Ss by means of TSTP as the cross-linker was evaluated. The SDM-Ms microspheres with smooth and porous morphology could be obtained. The SDM-Ms was changed from crystalline into amorphous structure after cross-linking and the adsorption capacity increased greatly. Surface-controlled erosion and interior rupture were the rate-limiting steps for degradation. The thermal stability of CSO was greatly improved after adsorption into the

SDM-Ms. The in vitro release of CSO from the SDM-Ms was initially rapid then followed by a slower release with diffusion, erosion, and degradation mechanisms. Therefore, Ss might be very useful as biodegradable polymers in developing a delivery system for controlled release and oxidative stability enhancement of CSO. Furthermore, SDM-Ms would provide a more effective and continuous application for bioactive agents in food and pharmaceutical industries.

Acknowledgments This research project was supported by the Programs of State Key Laboratory of Food Science and Technology of Nanchang University (SKLF-KF-201006, SKLF-TS-200818 and SKLF-MB-200809), the National 863 High Tech. Program of China (2008AA10Z332), the Department of Science and Technology of Shandong Province of China (2008GG20005005), and One Hundred Person Project of the Chinese Academy of Sciences (20090462).

References

1. Huang BW, Chiang MT, Yao HT, Chiang W (2005) The effect of adlay oil on plasma lipids, insulin and leptin in rat. Phytomedicine 12:433–439
2. Yu YL, Lu Y, Tang X, Cui FD (2008) Formulation, preparation and evaluation of an intravenous emulsion containing Brucea Javanica Oil and Coix Seed Oil for anti-tumor application. Biol Pharm Bull 31:673–680
3. Yu F, Gao J, Zeng Y, Liu CX (2008) Inhibition of Coix seed extract on fatty acid synthase, a novel target for anticancer activity. J Ethnopharmaco 119:252–258
4. Hu AJ, Zhao SN, Liang HH, Qiu TQ, Chen GH (2007) Ultrasound assisted supercritical fluid extraction of oiland coixenolide from adlay seed. Ultrason Sonochem 14:219–224
5. Woo JH, Li DP, Wilsbach K, Orita H, Coulter J, Tully E, Kwon TK, Xu S, Gabrielson E (2007) Coix seed extract, a commonly used treatment for cancer in china inhibits NFκB and protein Kinase C Signaling. Cancer Biol Ther 6:2005–2011
6. Lu Y, Zhang ZM, Zhang RH (1999) The study on antineoplastic effect of adlay seed oil. Pharm Clin Chin Trad Med 15:21–23
7. Freiberg S, Zhu XX (2004) Polymer microspheres for controlled drug release. Int J Pharm 282:1–18
8. Kumar N, Ravikumar MNV, Domb AJ (2001) Biodegradable block copolymers. Adv Drug Deliv Rev 53:23–44
9. Barbato F, Rotonda MIL, Maglio G, Palumbo R, Quaglia F (2001) Biodegradable microspheres of novel segmented poly (ether-ester-amide)s based on poly (ε-caprolactone) for the delivery of bioactive compounds. Biomaterials 22:1371–1378
10. Tietz M, Buettner A, Conde-Petit B (2008) Changes in structure and aroma release from starch-aroma systems upon α-amylase addition. Eur Food Res Technol 227:1439–1446
11. Xu Y, Ding WQ, Liu J, Li Y, Kennedy JF, Gu Q, Shao SX (2010) Preparation and characterization of organic-soluble acetylated starch nanocrystals. Carbohydr Polym 80:107–1084
12. Bourtoom T, Chinnan MS (2008) Preparation and properties of rice starchechitosan blend biodegradable film. LWT-Food Sci Technol 41:1633–1641
13. Mali S, Grossmann MVE (2003) Effects of yam starch films on storability and quality of fresh strawberries. J Agric Food Chem 24:7005–7011
14. Li BZ, Wang LJ, Li D, Chiu YL, Zhang ZJ, Shi J, Chen XD, Mao ZH (2009) Physical properties and loading capacity of starch-based microparticles crosslinked with trisodium trimetaphosphate. J Food Eng 92:255–260
15. Woo K, Seib PA (1997) Cross-linking of wheat starch and hydroxypropylated wheat starch in alkaline slurry with sodium trimetaphosphate. Carbohydr Polym 33:263–271
16. Hamdi G, Ponchel G, Duchene D (1998) An original method for studying in vitro the enzymatic degradation of cross-linked starch microspheres. J Controlled Release 55:193–201
17. Blanco MD, Sastre RL, Teijon C, Olmo R, Teijon JM (2006) Degradation behaviour of microspheres prepared by spray-drying poly (d, l-lactide) and poly (d, l-lactide-co-glycolide) polymers. Int J Pharm 326:139–147
18. Xiao YY, Song YM, Chen ZP, Ping QN (2006) Preparation of silymarin proliposome: a new way to increase oral bioavailability of silymarin in beagle dogs. J Pharm Sci 319:162–168
19. Peppas NA, Sahlin JJ (1989) Asimple equation for the description of solute release. III coupling of diffusion and relaxation. Int J Pharm 57:169–172
20. Yang YT, Wei XZ, Sun P, Wan JM (2010) Preparation, characterization and adsorption performance of a novel anionic starch microsphere. Molecules 15:2872–2885
21. Peng HL, Xiong H, Li JH, Xie MY, Liu YZ, Bai CQ, Chen LX (2010) Vanillin cross-linked chitosan microspheres for controlled release of resveratrol. Food Chem 121:23–28
22. Ispas-Szabo P, Ravenelle F, Hassan I, Preda M, Mateescu MA (2000) Structure-properties relationship in cross-linked high-amylose starch for use in controlled drug release. Carbohydr Res 323:163–175
23. Wang YL, Gao WY, Li X (2009) Carboxymethyl Chinese yam starch: synthesis, characterization, and influence of reaction parameters. Carbohydr Res 344:1764–1769
24. Soo PL, Cho J, Grant J, Ho E, Piquette-Miller M, Allen C (2008) Drug release mechanism of paclitaxel from a chitosan-ipid mplant system: effect of swelling, degradation and morphology. Eur J Pharm Biopharm 69:149–157
25. Peng HL, Xiong H, Li JH, Chen LX, Zhao Q (2010) Methoxy poly(ethylene glycol)-grafted-chitosan based microcapsules: synthesis, characterization and properties as a potential hydrophilic wall material for stabilization and controlled release of algal oil. J Food Eng 101:113–119